The Particle Finite Element Method for Multi-Fluid Flows

S.R. Idelsohn*, M. Mier-Torrecilla, J. Marti and E. Oñate

Abstract This paper presents the Particle Finite Element Method (PFEM) and its application to multi-fluid flows. Key features of the method are the use of a Lagrangian description to model the motion of the fluid particles (nodes) and that all the information is associated to the particles. A mesh connects the nodes defining the discretized domain where the governing equations, expressed in an integral form, are solved as in the standard FEM. We have extended the method to problems involving several different fluids with the aim of exploiting the fact that Lagrangian methods are specially well suited for tracking any kind of interfaces.

1 Introduction

Particle methods aim to represent the behavior of a physical problem by a collection of particles, where each particle moves accordingly to its own mass and the internal and external forces applied on it. All physical and mathematical properties are attached to the particle itself and not to the elements as in finite element methods (FEM). For instance, physical properties like viscosity or density, physical variables like velocity, temperature or pressure and also mathematical variables like gradients or volumetric deformations are assigned to each particle and they represent an average of the property around the particle position.

Particle methods are advantageous to treat discrete problems such as granular materials but also to treat continuous problems with internal interfaces in multi-fluid flows, frictional contact in fluid-solid interactions or free surfaces with breaking

S.R. Idelsohn · M. Mier-Torrecilla · J. Marti · E. Oñate
CIMNE International Center for Numerical Methods in Engineering, 08034 Barcelona, Spain;
e-mail: sergio@cimne.upc.edu

* ICREA Research Professor at CIMNE.

E. Oñate and R. Owen (eds.), *Particle-Based Methods*, Computational Methods in Applied Sciences 25, DOI 10.1007/978-94-007-0735-1_5,

waves. Particles are associated the different materials and thus the interfaces can be easily followed.

The most relevant characteristic of particle methods is that there is not a specified solution domain. The problem domain is defined by the particle positions. In order to evaluate the interacting forces between particles any classical approximation method may be used, including FEM, finite difference, meshless methods, etc. This means that a particle method may be used with or without a mesh, depending on the method chosen to evaluate the interacting forces.

Particle methods can be roughly classified in two types: (a) those based on probabilistic models, such as molecular dynamics, direct simulation Monte Carlo and lattice-gas automata; and (b) those based on deterministic models, such as SPH or other meshless methods, particle-mesh hybrid methods and the Particle Finite Element Method. The first class of methods represents macroscopic properties as statistical behavior of microscopic particles, so that a huge number of particles should be simulated for a long time to obtain accurate average values, while the second class of methods relies on the macroscopic Navier–Stokes equations.

This contribution is devoted to the Particle Finite Element Method and its application to multi-fluid flows. We introduce the basics of the method in Section 2, present the multi-fluid flow governing equations and their treatment with PFEM in Section 3, and illustrate the capabilities of the method in several examples in Section 4.

2 Particle Finite Element Method

The Particle Finite Element Method (PFEM) [20, 29] is a numerical technique for modeling and analysis of complex multidisciplinary problems in fluid and solid mechanics involving thermal effects, interfacial and free-surface flows, and fluid-structure interaction, among others.

PFEM is a particle method in the sense that the domain is defined by a collection of particles that move in a Lagrangian manner according to the calculated velocity field, transporting their momentum and physical properties (e.g. density, viscosity). The interacting forces between particles are evaluated with the help of a mesh. Mesh nodes coincide with the particles, so that when the particles move so does the mesh. On this moving mesh, the governing equations are discretized using the standard finite element method. The possible large distortion of the mesh is avoided through remeshing of the computational domain. Due to the fact that all the hydrodynamical information is stored in the nodes, remeshing does not introduce numerical diffusion. A robust and efficient Delaunay triangulation algorithm [13] (see Figure 1) allows frequent remeshing. This gives the method excellent capabilities for modeling large displacement and large deformation problems.

The particles are used to generate a discrete domain within which the integral form of the governing differential equations are solved. An algorithm is needed to define the boundary contours from the collection of particles. PFEM uses the alpha-

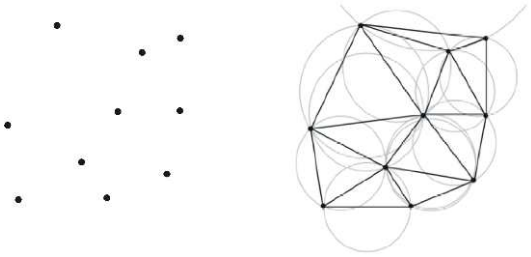

Fig. 1 Delaunay triangulation of a cloud of nodes

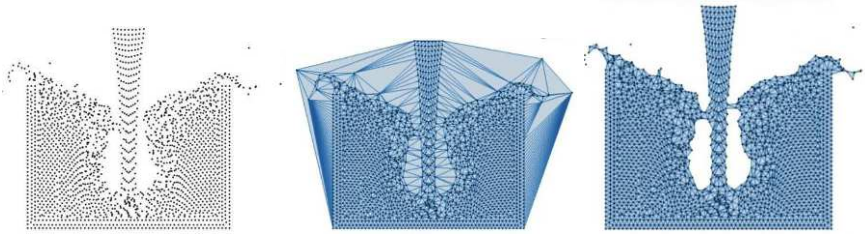

(a) (b) (c)

Fig. 2 Alpha-shape: (a) collection of nodes, (b) Delaunay triangulation of the convex hull, (c) mesh after alpha-shape

shape technique [6] to recognize the external boundary after the Delaunay triangulation of the domain convex hull (see Figure 2): All nodes defining an empty sphere with a radius $r(\mathbf{x})$ larger than $\alpha h(\mathbf{x})$ are considered to be boundary nodes. $h(x)$ is the distance between two neighboring nodes and the parameter α is chosen so that $\alpha \gtrsim 1$. Large values of α result in the convex hull of the collection, while small values return a boundary constituted just by the nodes. The error in the boundary surface definition is proportional to h. One of the advantages of the alpha-shape technique is the easy way to determine when particles separate from the fluid domain, as may happen in free surface problems (e.g. splashing).

- the information is particle-based, i.e. all the geometrical and mechanical information is attached to the nodes,
- the Lagrangian point of view for describing the motion,
- the equations are discretized and solved on a finite element mesh that is constructed at each time step,
- the boundaries of the domain are defined via the alpha-shape technique.

The use of a Lagrangian formulation eliminates the standard convection terms present in Eulerian formulations. These convection terms are responsible for non-linearity, non-symmetry and non-self-adjoin operators, which require the introduction of stabilization terms to avoid numerical oscillations. All these problems are absent in the Lagrangian formulation. Only the nonlinearity due to the unknown of

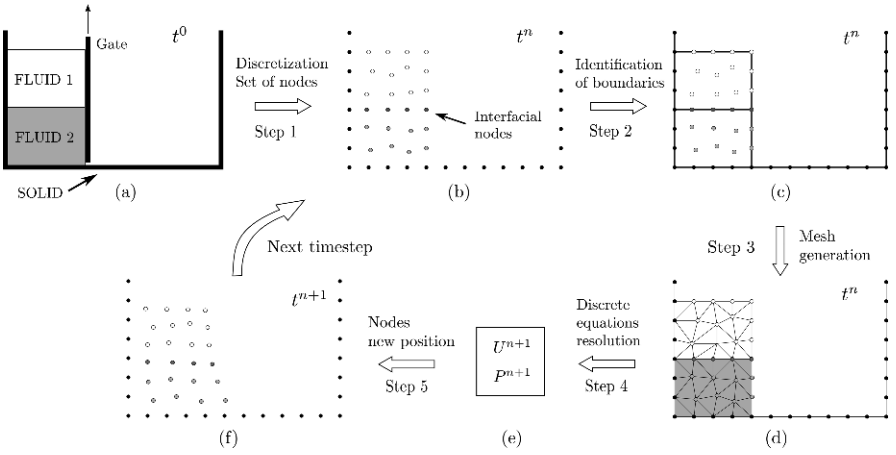

Fig. 3 PFEM solution steps illustrated in a simple dam break example. As the gate of the dam is removed the water begins to flow. (a) Continuous problem (b) Step 1, discretization in cloud of nodes at time t^n; (c) Step 2, boundary and interface recognition; (d) Step 3, mesh generation; (e) Step 4, resolution of the discrete governing equations; (f) Step 5, nodes moved to new position for time t^{n+1}

the final particle position remains. The resulting systems of equations are solved with a symmetric iterative scheme, such as the conjugate gradient method. Linear shape functions ($\mathbb{P}_1/\mathbb{P}_1$) are used for all unknowns. This equal order approximation for both the velocity and the pressure variables does not satisfy the inf-sup condition and therefore pressure stabilization is required.

A typical solution with the PFEM involves the following steps (illustrated in Figure 3):

1. The starting point at each timestep is the cloud of nodes in the fluid and solid domains.
2. Identification of the external boundary and the internal interfaces. The alpha-shape method is used for boundary definition.
3. Discretization of the domain with a finite element mesh generated by Delaunay triangulation.
4. Solution of the Lagrangian governing equations of motion for the fluid domain together with the boundary and interface conditions. Computing the relevant state variables at each timestep: velocities, pressure, temperature, and concentration.
5. Moving the mesh nodes to a new position in terms of the time increment and the velocity field computed in step (4).
6. Back to step (1) and repeat the solution process for the next timestep.

Thus PFEM combines the advantages of particle methods (namely only the "wet" domain considered, it is appropriate for changing domains, allows fluid fragmentation, tracks interfaces accurately, and does not introduce numerical diffusion when solving convection) with the accuracy of the finite element method.

Up to now, the method has been successfully applied to naval and coastal engineering [4, 20, 23, 28, 29], fluid-structure interaction [14–16, 21, 35], melting of polymers in fire [30], excavation problems [3], forming processes [8, 27] and multi-fluid flows [17, 18].

3 Multi-Fluid Flows

The simultaneous presence of multiple fluids with different properties in external or internal flows is found in daily life, environmental problems, and numerous industrial processes. Examples are fluid-fuel interaction in enhanced oil recovery, blending of polymers, emulsions in food manufacturing, rain droplet formation in clouds, fuel injection in engines, and bubble column reactors, to name only a few. Although multi-fluid flows occur frequently in nature and engineering practice, they still pose a major research challenge from both theoretical and computational points of view.

In the case of immiscible fluids, the dynamics of the interface between fluids plays a dominant role. The success of the simulation of such flows will depend on the ability of the numerical method to model accurately the interface and the phenomena taking place on it, such as the surface tension. The origin of the surface tension force lies in the different intermolecular attractive forces that act in the two fluids, and the result is an interfacial energy per area that acts to resist the creation of new interface, so that the interface behaves like a stretched membrane trying to minimize its area.

The main difference between a single-fluid (homogeneous) flow and a multi-fluid (heterogeneous) one is the presence of internal interfaces. In addition to the well-known difficulties in the simulation of homogeneous flows (namely the coupling of pressure and velocity through the incompressibility constraint, the need of the discretization spaces to satisfy the inf-sup condition, and the non-linearity of the governing equations), numerical methods for multi-fluid flows face the following challenges:

1. Accurate definition of the interface position.
   The interface separating the fluids needs to be tracked accurately without introducing excessive numerical smoothing.
2. Modeling the jumps in the fluid properties across the interface.
   Large jumps of fluid density and viscosity across the interface need to be properly taken into account in order to satisfy the momentum balance at the vicinity of the interface.
3. Modeling the discontinuities of the flow variables across the interface.
   Velocity and pressure may be discontinuous across the interface under certain conditions.
4. Modeling the surface tension.
   Since surface tension plays a very important role in the immiscible interface dynamics, this force needs to be accurately evaluated and incorporated into the model.

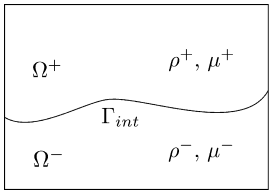

Fig. 4 Two-fluid flow configuration

The computation of multi-fluid flows requires to solve, besides the governing equations in each fluid, all the physical phenomena the interface may be subject to, such as surface tension, thermal diffusion, chemical diffusion, phase change or chemical reactions, and to model interface topology changes like breakup or coalescence.

3.1 Governing Equations

Let $\Omega \subset \mathbf{R}^d$, $d \in \{2, 3\}$, be a bounded domain containing two different fluids (see Figure 4). We denote time by t, the Cartesian spatial coordinates by $\mathbf{x} = \{x_i\}_{i=1}^d$, and the vectorial operator of spatial derivatives by $\boldsymbol{\nabla} = \{\partial_{x_i}\}_{i=1}^d$. The evolution of the velocity $\mathbf{u} = \mathbf{u}(\mathbf{x}, t)$ and the pressure $p = p(\mathbf{x}, t)$ is governed by the Navier–Stokes equations:

$$\rho \frac{\mathrm{d}\mathbf{u}}{\mathrm{d}t} = \nabla \cdot \sigma + \rho \mathbf{g} \quad \text{in } \Omega \times (0, T) \tag{1a}$$

$$\frac{\mathrm{d}\rho}{\mathrm{d}t} + \rho \nabla \cdot \mathbf{u} = 0 \quad \text{in } \Omega \times (0, T) \tag{1b}$$

where ρ is the density, σ the Cauchy stress tensor, $\mathbf{g}$ the vector of gravity acceleration, and $\mathrm{d}\phi/\mathrm{d}t$ represents the total or material derivative of a function ϕ. The constitutive equation for a Newtonian and isotropic fluid takes the form

$$\sigma = -p\mathbf{I} + 2\mu\left(\mathbf{D} - \frac{1}{3}\varepsilon_V \mathbf{I}\right) \tag{2}$$

with $\mathbf{I}$ the identity tensor, μ the dynamic viscosity, $\mathbf{D} = \frac{1}{2}(\nabla \mathbf{u} + \nabla^T \mathbf{u})$ the strain rate tensor, and $\varepsilon_V = \nabla \cdot \mathbf{u}$ the volumetric strain rate.

Let $\Gamma_{\text{int}}(t)$ be the interface that cuts the domain Ω in two open subdomains, $\Omega^+(t)$ and $\Omega^-(t)$, which satisfy: $\Omega^+ \cap \Omega^- = \emptyset$, $\Omega = \bar{\Omega}^+ \cup \bar{\Omega}^-$, and $\Gamma_{\text{int}} = \bar{\Omega}^+ \cap \bar{\Omega}^- = \partial\Omega^+ \cap \partial\Omega^-$. In each subdomain, the physical properties are defined as:

$$\rho = \rho(\mathbf{x}, t) = \begin{cases} \rho^+ \text{ if } \mathbf{x} \in \Omega^+(t) \\ \rho^- \text{ if } \mathbf{x} \in \Omega^-(t) \end{cases}, \qquad \mu = \mu(\mathbf{x}, t) = \begin{cases} \mu^+ \text{ if } \mathbf{x} \in \Omega^+(t) \\ \mu^- \text{ if } \mathbf{x} \in \Omega^-(t) \end{cases} \tag{3}$$

If density and viscosity are assumed to remain constant in each fluid (i.e. fluids are incompressible, immiscible, and isothermal), we have that $\mathrm{d}\rho/\mathrm{d}t = 0$ and $\mathrm{d}\mu/\mathrm{d}t = 0$. Consequently, we have on the one side that $\varepsilon_V = \nabla \cdot \mathbf{u} = 0$, this is the mass conservation equation for incompressible flows; and on the other side, that $(\mathrm{d}/\mathrm{d}t)\,\Gamma_{\text{int}} = 0$. This latter consequence means that interfaces are material surfaces, which move with the fluid velocity $\mathbf{u}$, and therefore, they are naturally tracked in Lagrangian formulations.

Boundary and interface conditions

In order for the Navier–Stokes problem (1) to be well posed, suitable boundary conditions need to be specified. On the external boundary $\partial\Omega = \Gamma_D \cup \Gamma_N$, such that $\Gamma_D \cap \Gamma_N = \emptyset$, we consider the following:

$$\mathbf{u} = \bar{\mathbf{u}} \quad \text{on } \Gamma_D \tag{4}$$

$$\sigma \cdot \mathbf{n} = \bar{\sigma}_n \quad \text{on } \Gamma_N \tag{5}$$

$\bar{\mathbf{u}}$ is the prescribed velocity, $\mathbf{n}$ the outer unit normal to Γ_N, and $\bar{\sigma}_n$ the prescribed traction vector. A Neumann boundary Γ_N with $\bar{\sigma}_n = \mathbf{0}$ is called *free surface*.

On the internal interfaces Γ_{int}, the coupling conditions are [1]:

$$[\![\mathbf{u}]\!] = \mathbf{0} \quad \text{on } \Gamma_{\text{int}} \tag{6}$$

$$[\![\sigma]\!] \cdot \mathbf{n} = \gamma\kappa\mathbf{n} \quad \text{on } \Gamma_{\text{int}} \tag{7}$$

with $\mathbf{n}$ now the unit normal to Γ_{int}, γ the surface tension coefficient, κ the interface curvature, and $[\![\phi]\!] = \phi^+ - \phi^-$ represents the jump of a quantity ϕ across the interface.

Equation (6) expresses the continuity of all velocity components. The normal component has to be continuous when there is no mass flow through the interface, and the tangential components have to be continuous when both fluids are viscous ($\mu^+, \mu^- > 0$), similar to a no-slip condition.

Equation (7) expresses that the jump in the normal stresses is balanced with the surface tension force. This force is proportional to the interface curvature and points to the center of the osculating circle that approximates Γ_{int}. The surface tension coefficient γ is assumed constant and its value depends on the two fluids at the interface.

3.2 Discontinuities at the Interface

Discontinuities at the interface can be of two types:

- $\mathcal{C}^0$ *discontinuity*, when the flow variable has a kink (i.e. the gradient has a jump), and

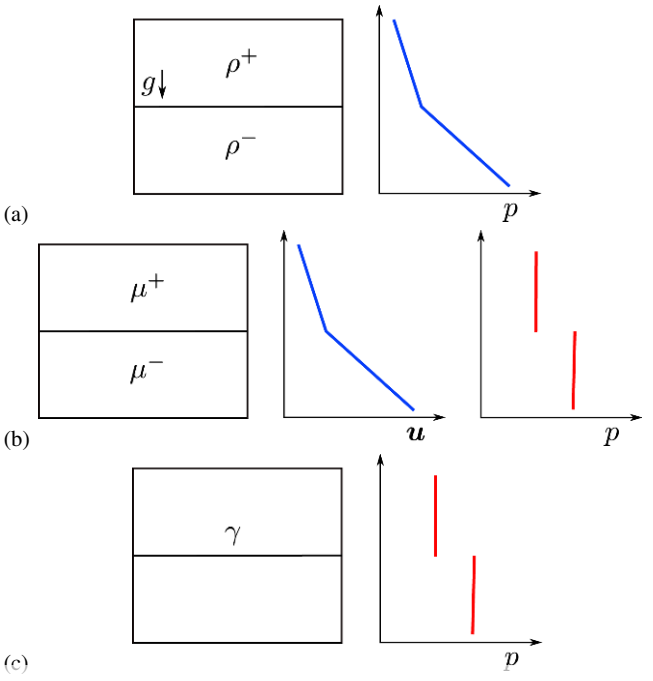

Fig. 5 Flow discontinuities for: (a) density jump, (b) viscosity jump, and (c) surface tension

- $\mathcal{C}^{-1}$ *discontinuity*, when the flow variable itself has a jump.

Differences in density at the interface cause a kink in the hydrostatic pressure profile, leading to a jump in the pressure gradient, and then to a $\mathcal{C}^0$ discontinuity in the pressure field (Figure 5a).

Differences in viscosity lead to discontinuous components of the strain rate tensor $\mathbf{D}$, and therefore to a $\mathcal{C}^0$ discontinuity of the velocity field at the interface (Figure 5b):

$$\mathbf{t}\cdot[\![\sigma]\!]\cdot\mathbf{n}=0 \quad\Longrightarrow\quad \mu^+\left(\frac{\partial u_t}{\partial n}+\frac{\partial u_n}{\partial s}\right)^+-\mu^-\left(\frac{\partial u_t}{\partial n}+\frac{\partial u_n}{\partial s}\right)^-=0 \tag{8}$$

with $\partial_s=\mathbf{t}\cdot\nabla$ the tangential derivative.

Both differences in viscosity and the presence of surface tension cause a $\mathcal{C}^{-1}$ discontinuity in the pressure field (Figures 5b and 5c), as shown in [17]:

$$\mathbf{n}\cdot[\![\sigma]\!]\cdot\mathbf{n}=\gamma\kappa \quad\Longrightarrow\quad p^+-p^-=2(\mu^+-\mu^-)\frac{\partial u_n}{\partial n}-\gamma\kappa \tag{9}$$

Notice that even in the case of $\gamma=0$, pressure is discontinuous when $\mu^+\neq\mu^-$.

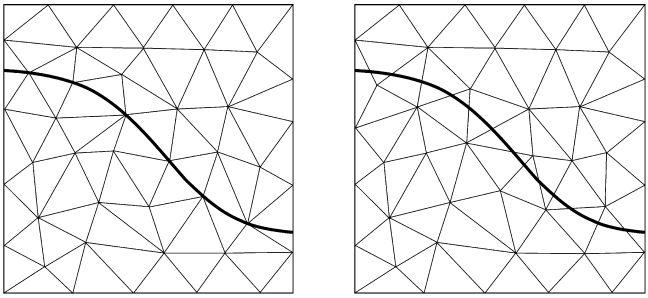

Fig. 6 (a) Moving mesh adapted to the interface, and (b) fixed mesh, where interface moves through the elements

3.3 Interface Description

A major challenge in the simulation of interfaces between different fluids is the accurate description of the interface evolution. The location of the interface is in general unknown and coupled to the local flow field which transports the interface. It is essential that the interface remains sharp along time and is able to fold, break and merge. In the past decades a number of techniques have been developed to model interfaces in multi-fluid flow problems, each technique with its own particular advantages and disadvantages. Comprehensive reviews can be found in e.g. [2, 36, 37, 40].

The main classification of interface descriptions is regarding the reference frame adopted (see Figure 6). In the *moving mesh methods*, the mesh is deformable and adapted to the interface, which is explicitly tracked along the trajectories of the fluid particles. Examples are methods based on the Arbitrary Lagrangian-Eulerian (ALE) formulation [12, 33], the deformable-spatial-domain/stabilized space-time deformation (DSD/SST) method [38, 39], or the fully Lagrangian formulation such as in [10, 34] and the Particle Finite Element Method [4, 19, 20, 22].

On the other hand, *fixed mesh methods* use a separate procedure to describe the position of the interface. They can be further grouped in *front-tracking methods*, which use massless marker points to follow the fluid interface while the Navier–Stokes equations are solved on a fixed mesh [9, 41], and *front-capturing methods*, which introduce a new variable ψ in the model to describe the presence or not of a fluid in a position of the domain. The most extended front-capturing methods are the Volume-of-Fluid, originally developed by Hirt [11], and the Level Set method by Osher et al. [31].

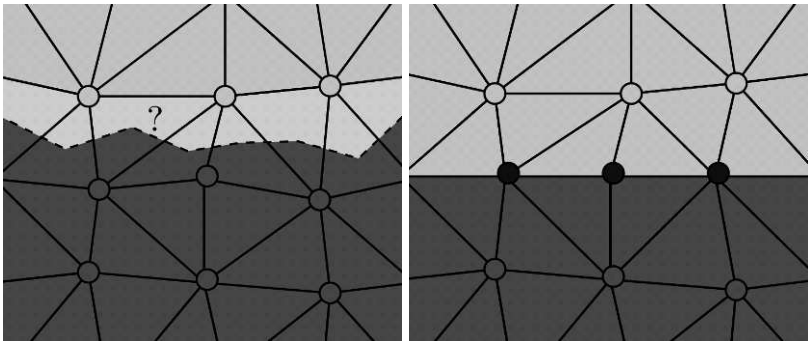

(a) Interface across elements (b) Nodal interface

Fig. 7 Possible interface representations in PFEM: (a) interface across elements for miscible fluids, (b) nodal interface (with interfacial nodes in black) for immiscible fluids

3.4 PFEM for Multi-Fluid Flows

One of the features of particle methods is that all the physical properties are attached to the nodes instead of to the elements. The mesh is frequently updated and hence, it is difficult to keep physical properties at the element level. Multi-fluid flows can have a jump in the fluid properties of several orders of magnitude. One must decide where does the internal interface between two different fluids occur. The typical solution for a particle method would be to have the interface inside the elements sharing particles with different densities so that, at the element integration point k, density takes the mean value

$$\rho_k = \frac{1}{nv} \sum_{a=1}^{nv} \rho_a$$

(where nv is the number of nodes of the element). We call this possibility *interface across elements* (Figure 7a). Another possibility is to impose that the interface between different materials is described by element edges. This is called *nodal interface* (Figure 7b). For the nodal interface one must accept that elements sharing particles with two different densities have one or the other particular density value. Now, the density at the element integration point k takes the value

$$\rho_k = \begin{cases} \rho^+ \text{ if } k \in \Omega^+ \\ \rho^- \text{ if } k \in \Omega^- \end{cases} \tag{10}$$

Both possibilities have advantages and disadvantages. Interfaces across elements are more stable as they do not change much when remeshing is performed but on the other hand, nodal interfaces are more accurate because they allow to represent exactly the jumps in the physical properties and the discontinuities of the flow variables, as illustrated in Figure 8.

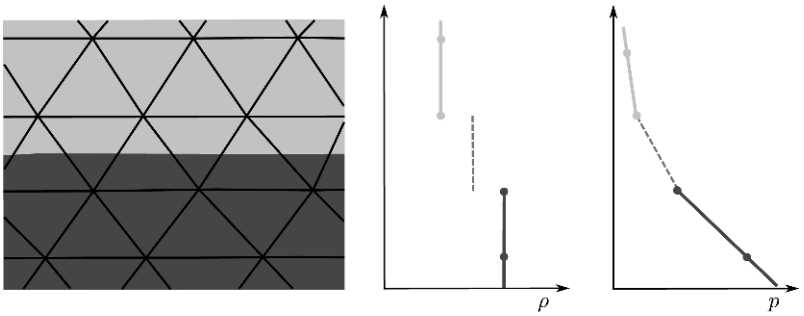

(a) Interface across elements

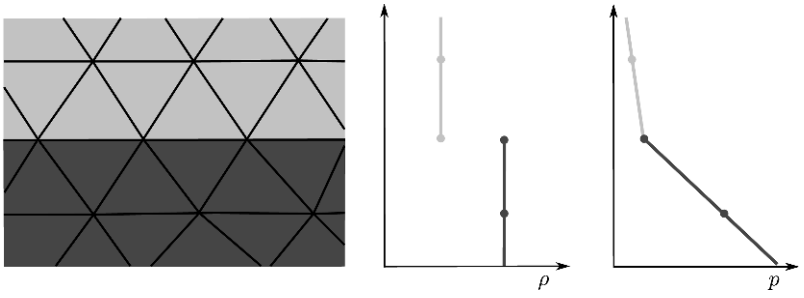

(b) Nodal interface

Fig. 8 Density and pressure representations for the different interface definitions: in the interface across elements (a), standard linear elements cannot represent accurately the pressure weak discontinuity; while in the nodal interface (b) the representation is exact

We mainly focus on immiscible multi-fluid flows to exploit the fact that Lagrangian methods are able to track interfaces in a natural and accurate way. For this purpose, we use the nodal interface, and since in this representation the interface is described by mesh nodes and element edges, it is a well-defined curve and the information regarding its location and curvature is readily available. The interface nodes carry the jump of properties (e.g. density, viscosity), maintaining the interface sharp without diffusion along time. Furthermore, it is straightforward to impose the on the interface and to treat any number of fluids. Therefore in PFEM the interface is tracked accurately without introducing numerical smoothing (challenge 1).

Regarding the modeling of the jumps in the fluid properties across the interface (challenge 2), while in fixed mesh methods typically the interface is considered to have a finite thickness and the fluid properties change smoothly and continuously from the value on the one side of the interface to the value on the other side, PFEM treats the interface in a sharp manner, so that it is clear which property value is valid at each point.

Regarding the modeling of the discontinuities in the flow variables across the interface (challenge 3), in fixed mesh methods where the physical properties have been smoothed, functions are continuous across the interface and thus not appropri-

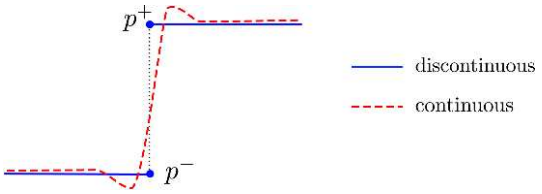

Fig. 9 Pressure profiles when using continuous and discontinuous representations

ate for the approximation of discontinuous variables. When the physical properties are modeled sharp, the elements cut by the interface require a special treatment in order to be able to represent the discontinuities. Gravity dominated flows will require "enrichment" of the pressure approximation, and viscosity dominated flows will require "enrichment" of the velocity approximation. On the contrary, $\mathcal{C}^0$ discontinuities need no special attention when the interface is aligned with the mesh, as the kinks in the solution are automatically represented. Only $\mathcal{C}^{-1}$ discontinuities need some attention in PFEM. In particular, the pressure field has been made double-valued at the interface, i.e. pressure degrees of freedom have been duplicated (p^+, p^-) in the interface nodes [17]. The pressure discontinuity caused by the jump in viscosity and/or surface tension (Eq. (9)) is thus optimally approximated. Figure 9 shows that the use of continuous pressure representations may introduce errors in the incompressibility condition.

Moreover, stabilization is needed in incompressible flows when interpolation spaces for velocity and pressure do not satisfy the inf-sup condition. Many stabilization procedures have been proposed in the literature, such as the Streamline-Upwind/Petrov-Galerkin, Galerkin Least-Squares, Finite Calculus, or Orthogonal Sub-Scale methods. Those that include the projection of the pressure gradient need to be modified when density changes at the interface to take into account the variation of the hydrostatic pressure gradient. In PFEM the pressure gradient projection is modeled discontinuous to take into account the jump in density. For details, refer to [18, 24].

Regarding the modeling of the surface tension force $\mathbf{f}_{st} = \gamma\kappa\mathbf{n}$ at immiscible interfaces (challenge 4), this force is naturally incorporated in the weak form of the momentum equation in the finite element method. There are several ways to calculate the curvature κ from the information of the interface location. The one we follow in PFEM is based on the *osculating circle* of a curve, which is defined as the circle that approaches the curve most tightly among all tangent circles at a given point. From the radius of the osculating circle, the quantity $\kappa\mathbf{n}$ required for $\mathbf{f}_{st}$ is calculated as (see Figure 10):

$$\mathbf{n} = \frac{\mathbf{R}}{|\mathbf{R}|}, \qquad \kappa\mathbf{n} = \frac{\mathbf{R}}{|\mathbf{R}|^2} \tag{11}$$

Details on the accuracy of the surface tension computation have been given in [26].

The accuracy of the curvature calculation is improved by refining the mesh close to the interface. By means of a distance function, we prescribe an element size which is fine at the interface and coarse far away. This allows us to use arbitrarily

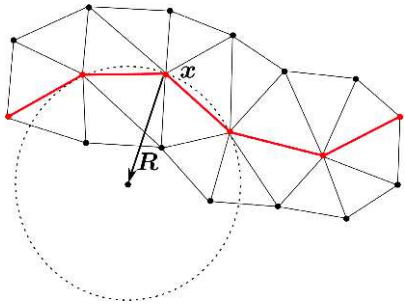

Fig. 10 Calculation of the osculating circle at node **x**

fine meshes without increasing the total number of elements to impractical values as it would be the case with a uniform mesh.

3.5 Combustion Problem

Within the flows labeled as multi-fluid there are the fluid-combustible interaction problems mentioned before. These problems are important for materials such as the polymers, which are characterized by their strength, low cost, and easy processability, with applications ranging from packaging to injection of molded parts or structural components. The behavior of polymers in fire is therefore of great interest due to their role in the ignition and stages of fire growth. of these problems is due some materials with characteris as the strength, low cost, and easy processability has been used as polymers, with applications ranging from packaging to injection of molded parts to structural components. Their behaviour in fire is therefore of considerable interest because they play an important role in the ignition and stages of fire growth.

When a polymer is heated, it starts to be pyrolysed while ejecting volatile gases [5]. The fluid above the solid fuel provides a region where the combustion reaction can take place. Once the pyrolysis products are released from the surface, they are able to mix with the surrounding air while being heated from the nearby flame. The rate of fuel consumption depends on both the reaction rate and the speed at which fuel and oxidized are mixed. Once heated to ignition, oxidation of the gaseous fuel leads to the generation of combustion products. The intermediates and final products of the combustion are a complex function of the reaction rates and local conditions.

Solving the combustion problem means to solve for the flow together with the chemical species. Therefore the Navier–Stokes equations (1) apply for the multi-species multi-reaction gas but they require the following additional equations:

$$\rho C \frac{\mathrm{d}T}{\mathrm{d}t} = \nabla \cdot (\kappa \nabla T) \quad \text{in } \Omega \times (0, T) \tag{12}$$

$$\rho \frac{\mathrm{d}Y_k}{\mathrm{d}t} = w_k + \nabla \cdot (\mathcal{D}\rho \nabla Y_k) \quad \text{in } \Omega^+ \times (0, T) \tag{13}$$

where $T = T(\mathbf{x}, t)$ is the temperature, $Y_k = Y_k(\mathbf{x}, t)$ the mass fraction of species k, C the heat capacity, κ the thermal conductivity, w_k the source term of specie k and $\mathcal{D}$ the diffusion coefficient.

The coupling between temperature and velocity will be considered by introducing the Boussinesq approximation.

The mass fractions Y_k are defined by

$$Y_k = \frac{m_k}{m} \tag{14}$$

where m_k is the mass of species k present in a given volume Ω^+ and m is the total mass of gas for this volume. Obviously, the sum of mass fractions must be

$$\sum Y_k = 1 \tag{15}$$

for $k = 1$ to N, where N is the number of species in the reacting mixture.

Let $\Omega^+(t)$ represent the fluid and $\Omega^-(t)$ the combustible. In each subdomain, the physical properties are defined as

$$C(\mathbf{x}, t) = \begin{cases} C^+ \text{ if } \mathbf{x} \in \Omega^+(t) \\ C^- \text{ if } \mathbf{x} \in \Omega^-(t) \end{cases}, \quad \kappa(\mathbf{x}, t) = \begin{cases} \kappa^+ \text{ if } \mathbf{x} \in \Omega^+(t) \\ \kappa^- \text{ if } \mathbf{x} \in \Omega^-(t) \end{cases},$$

$$\mathcal{D}(\mathbf{x}, t) = \begin{cases} \mathcal{D}^+ \text{ if } \mathbf{x} \in \Omega^+(t) \\ 0 \quad \text{if } \mathbf{x} \in \Omega^-(t) \end{cases} \tag{16}$$

and the boundary condition at the interface is the following:

$$-\rho \mathcal{D} \frac{\partial Y_F}{\partial n} = f(T)(1 - Y_F) \tag{17}$$

In the present study, the polymer/air reactive system is modeled as a simplified one-step chemical reaction between the fuel (F) and the oxidizer (O)

$$F + s\,O \rightarrow (1 + s)\,\text{Products} \tag{18}$$

where s is the stoichiometric ratio [32]. These species are identified by their mass fractions Y_F, Y_O and Y_P. Species reaction rates w_k are all related to the single-step reaction rate [42]

$$w_m = -B \frac{1}{T^2} Y_F Y_O e^{-(E/R\,T)} \tag{19}$$

where B, E and R are appropiate constants and the temperature T. So the oxidizer and product reaction rates are linked to the fuel reaction rate

$$w_O = (s) w_m \tag{20}$$

$$w_P = (1 + s) w_m \tag{21}$$

and the heat realease per unit of volume from combustion is therefore scaled according to

$$Q = -w_m \, \Delta H \quad \text{in } \Omega^+ \tag{22}$$

where ΔH is the heat of combustion. The value of Q is introduced as a source term in Eq. (12).

The effect of gasification can be introduced by adding a (nonlinear) energy loss term in Eq. (12). This term represents the energy that migrates from the system to the gas due to the gasification of a part of the material during the heating process. The gasification heat flux has the following form:

$$q_{\text{gas}} = H \varepsilon_v \quad \text{in } \Omega^- \tag{23}$$

with H being the heat of degradation and $\varepsilon_v = f(T)$, where $f(T)$ expresses the relation between the volume variation due to the temperature ε_v and the temperature itself. In our work the following Arrhenius function has been chosen [7]:

$$f(T) = -\rho A e^{-E/RT} \tag{24}$$

The computed mass loss has to be included in the problem to ensure that the volume variation of the sample is correctly modeled. This term is positive in Ω^+ because it represents the conversion rate from solid to gases due to evaporation, devolatization and heterogeneous reactions, and thus negative in Ω^-.

4 Numerical Examples

The Particle Finite Element Method described here has been tested in several multi-fluid flow problems (such as the two-fluid sloshing [18], extrusion of viscous fluids [17] and bubble rise [26]), and fluid-structure interaction problems where the structure is modeled as a viscous fluid [15, 16]. In this section we show the capability of PFEM to handle interfaces with changing topology in flows with surface tension and to model combustion flows.

Topology changes in multi-fluid flows can be divided into two classes:

(a) Films that fragment. If a bubble approaches a flat surface or another bubble, the fluid in between must be squeezed out before the bubbles are sufficiently close so that the film becomes unstable to attractive forces and fragment.
(b) Threads that break. A long and thin cylinder of fluid will generally break by the Plateau–Rayleigh instability in the region where the cylinder becomes sufficiently thin so that surface tension pinches it into two.

We have simulated an example of each class: (a) the breakup of a bubble in Section 4.1 and (b) the breakup of an injected fluid in Section 4.2. The last numerical example deals about melting and combustion of a candle (Section 4.3).

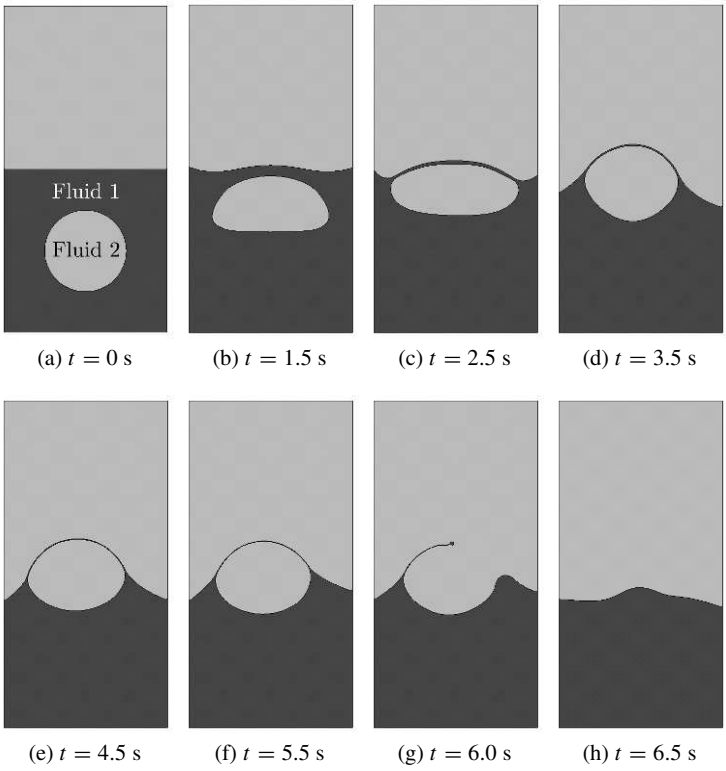

(a) $t = 0$ s (b) $t = 1.5$ s (c) $t = 2.5$ s (d) $t = 3.5$ s

(e) $t = 4.5$ s (f) $t = 5.5$ s (g) $t = 6.0$ s (h) $t = 6.5$ s

Fig. 11 Bubble breakup

4.1 Bubble Breakup

The problem consists in a bubble rising in a liquid column as illustrated in Figure 11a [26]. We consider a rectangular domain $(0, 1) \times (0, 2)$ with a flat interface at $y = 1$ and a circular bubble centered at $(0.5, 0.5)$ and radius equal to 0.25. The physical properties of the fluids are: $\rho_1 = 1000$, $\rho_2 = 100$, $\mu_1 = 10$, $\mu_2 = 1$, $g = 0.98$, and $\gamma = 24.5$.

The bubble rises due to buoyancy, approaching the flat interface. The film of heavy fluid that separates the two regions of light fluid becomes thinner and thinner until it fragments and the regions fuse (Figure 11). Whereas in the physical reality the fragmentation of the film is caused by attractive forces at the microscopic scale (forces which are usually not included in the continuum description), in our simulations fragmentation is caused by a connectivity change at the interface, as illustrated in Figure 12.

One of the main difficulties we face in our Lagrangian approach is the connectivity changes introduced by the remeshing process. In general, these reconnections may alter the equilibrium at the interface, slow down convergence and affect mass

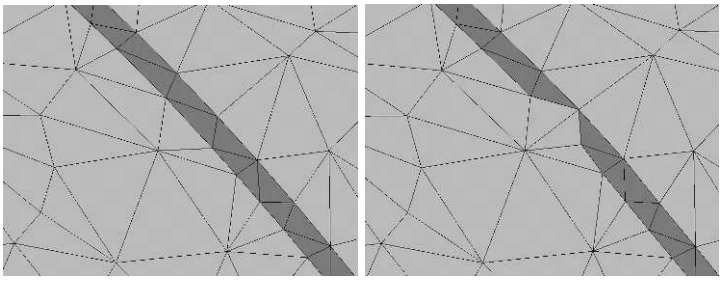

(a) t^n (b) t^{n+1}

Fig. 12 Connectivity change that produces breakup at fluid films spanned by just one mesh element

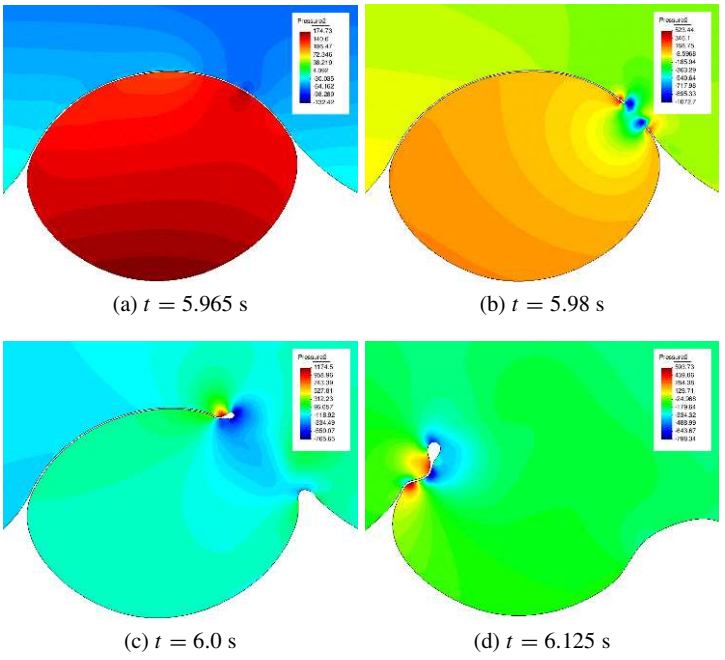

(a) $t = 5.965$ s (b) $t = 5.98$ s

(c) $t = 6.0$ s (d) $t = 6.125$ s

Fig. 13 Pressure field at breakup (variable scale ranges in legend)

conservation. Thus, in interfacial flows it is essential to avoid them. We are using an unconstrained Delaunay triangulator which does not allow to fix connectivities. Therefore, to ensure that a specific connectivity remains, we refine long interfacial edges and remove nodes too close to the interface. Unfortunately, this strategy would preclude the possibility of breakup, as the interface could elongate endlessly. In the way PFEM defines interfaces, it is possible to have fluid regions spanned by just one element layer (Figure 12). The *breakup criterium* we have implemented in PFEM is to permit connectivity changes in elements where all nodes lie at the interface. In this way, a thin fluid thread can stop elongating and fragment. Breakup is then

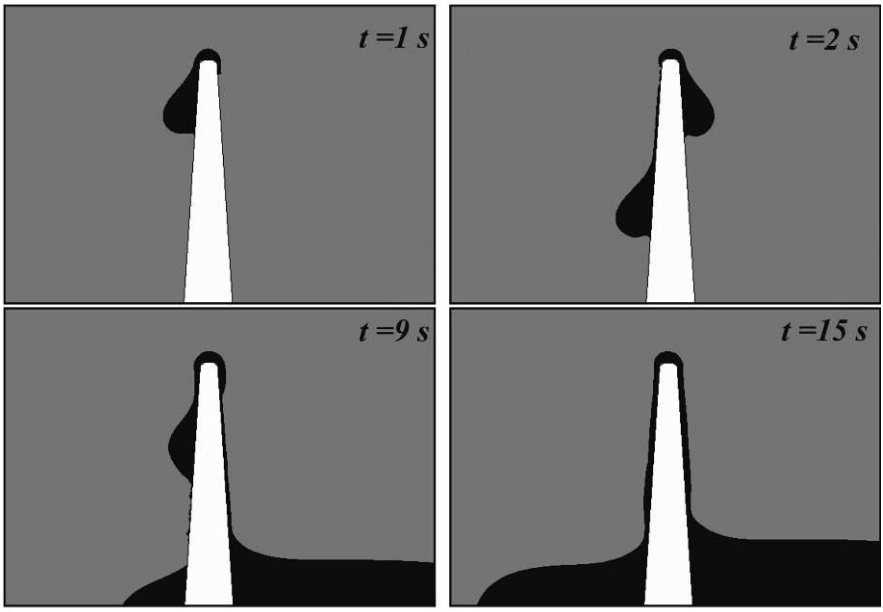

Fig. 14 Flow evolution for $\mathbf{u}_j = 0.025$ m s^{-1} ($Fr = 0.6$, $Re = 44$)

dependent on the mesh resolution, that is, it happens when the thickness of the film is similar to the mesh resolution of the interface. This is not a drawback specific of PFEM, breakup is mesh dependent in front-capturing methods as well. For example, in the level set method, two interfaces are described as two different zero contours of the same level set function, and these interfaces will automatically merge once they get close enough, relative to the spatial resolution of the mesh where the level set function is defined.

The pressure field at breakup is shown in Figure 13. The different pressure values inside and outside the bubble equilibrate after breakup, what occurs at $t = 5.97$ s.

4.2 Negatively Buoyant Jet

Negatively buoyant jets consist in a dense fluid injected vertically upward into a lighter fluid. The jet momentum is continually being decreased by buoyancy forces until the vertical velocity becomes zero. The jet then reaches its maximum penetration height, reverses direction and flows back. This problem has been experimentally and numerically studied in [25].

We consider the injection of water ($\rho_w = 1000$ kg m^{-3}, $\mu_w = 10^{-3}$ Pa s) through a nozzle in the base of a tank containing oil ($\rho_o = 900$ kg m^{-3}, $\mu_o = 200 \times 10^{-3}$ Pa s).

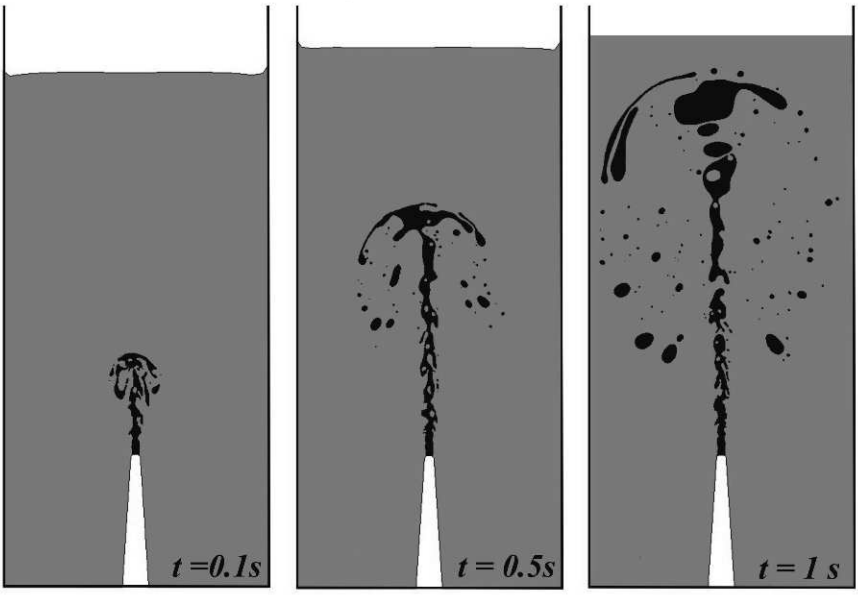

Fig. 15 Flow evolution for $\mathbf{u}_j = 1$ m s^{-1} ($Fr = 28$, $Re = 1310$)

For negatively buoyant jet flows with very low Froude (Fr, inertia vs. buoyancy) and Reynolds (Re, inertia vs. viscosity) numbers, the injected fluid reaches an almost constant maximum height, as shown in Figure 14. At higher velocities at the nozzle (i.e. higher Fr and Re numbers), the jet begins to oscillate between a maximum and a minimum height, and over a certain threshold, instabilities at the interface cause the jet to break into droplets (see Figure 15).

4.3 Candle Combustion

The problem considered here is a two-dimensional burning rod inside a closed contanier, as illustred in Figure 16a. For simplicity, we will refer to this object as a "candle". The dimensions of the candle are 50 cm high by 5 cm thick. From time $t = 0$ to $t = 10$ s, the temperature at the candle top is set to 950 K. In the solid phase, the processes of heating and gasification take place. Simultaneously, in the gas phase chemical processes are initiated, and temperature, fuel and oxidizer concentration gradients develop. The pysical properties are $\rho_1 = 1$ kg m^{-3}, $\rho_2 = 1170$ kg m^{-3}, $\mu_1 = 0.001$ Pa s, $\mu_2 = 10^6$ Pa s, $\mathcal{D} = 10^{-5}$ m^2 s^{-1}. Figures 16 to 18 show snapshots of the temperature evolution and the flame zone in time for all configurations. Notice that as the flame grows (see Figures 17 and 18) the combustion takes place in a larger area. Finally, the flame is extinguished, first in the configuration in

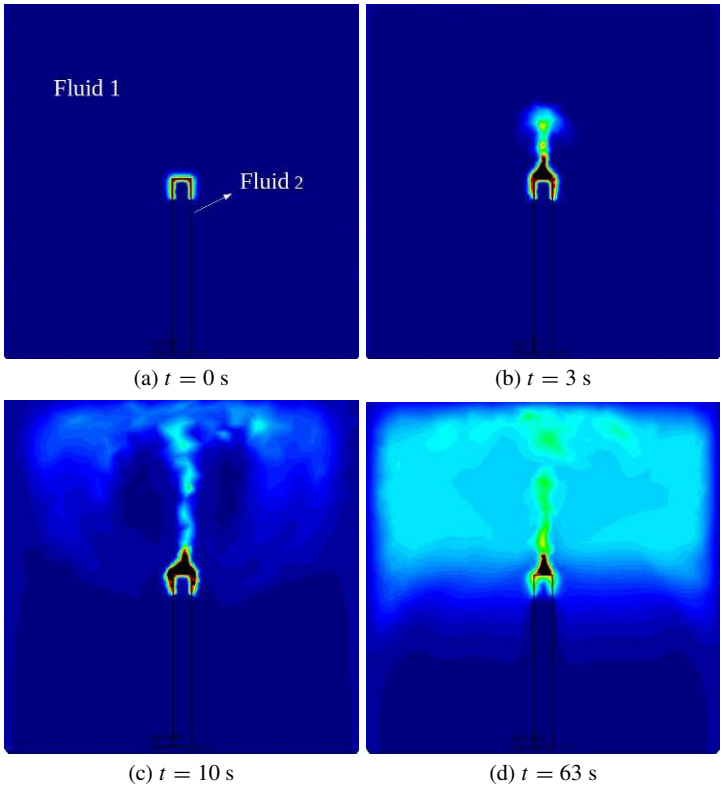

Fig. 16 Temperature evolution in the combustion of a vertical (bottom-up) candle

Figure 16 and later in the other examples, when reactions stop due to the particles of non-oxygenated air returning to the combustion zone.

In the next example, the material properties for the candle are the same as in the previous example. The temperature increases in the candle due to heat of combustion, and the viscosity decreases by several orders of magnitude as a function of temperature [30]. This induces the melting and flow of the candle material in the heated zone. The melt flows down along the heated face of the sample and drips onto the surface below. Figures 19 and 20 show the progressive melting of the candle exposed to the heat from combustion, along with the change of the flame shape. The dripping material transports the flame (see Figure 19c) and continues burning on the surface below. After some seconds, the candle falls down and the flame is extinguished.

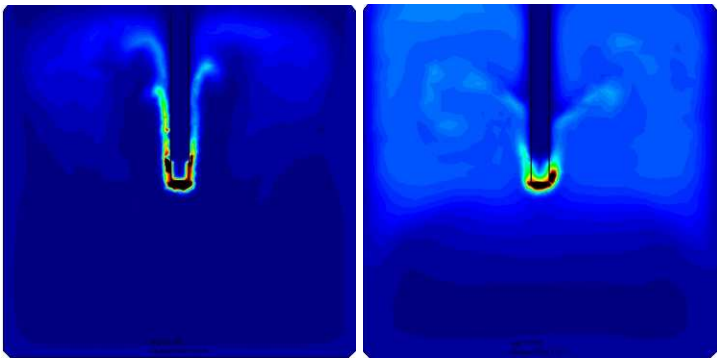

(a) $t = 12$ s (b) $t = 75$ s

Fig. 17 Temperature evolution in the combustion of a vertical (top-down) candle

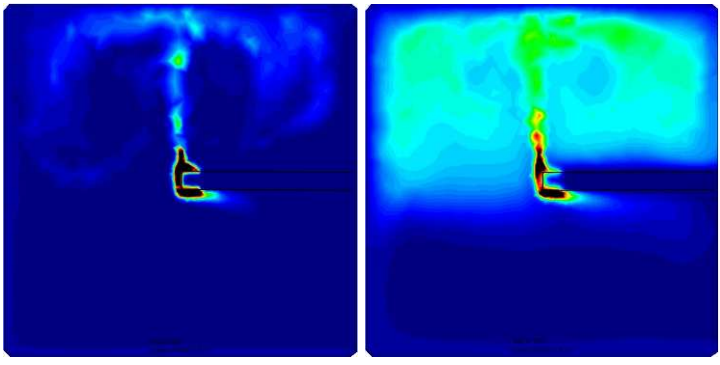

(a) $t = 7$ s (b) $t = 41$ s

Fig. 18 Temperature evolution in the combustion of a horizontal candle

5 Summary and Conclusions

The Particle Finite Element Method (PFEM) has been used to solve the incompressible Navier–Stokes equations for heterogeneous fluid flows (such as the rising bubble, extrusion of materials with different viscosity and candle combustion with melting and dripping). The results show the ability of the method to deal with problems from the simple case of fluids with a single interface to the case of strong mixed fluids with multiple interfaces. Problems with a big difference between the two materials were also performed without showing any instability.

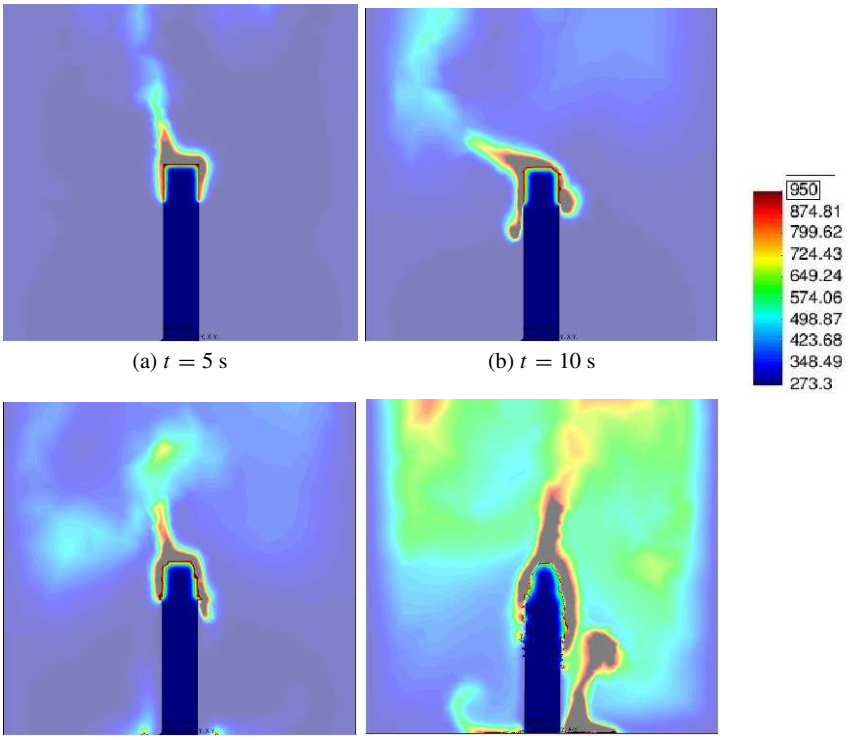

(a) $t = 5$ s (b) $t = 10$ s

(c) $t = 12$ s (d) $t = 25$ s

Fig. 19 Melting and dripping of a candle: temperature evolution

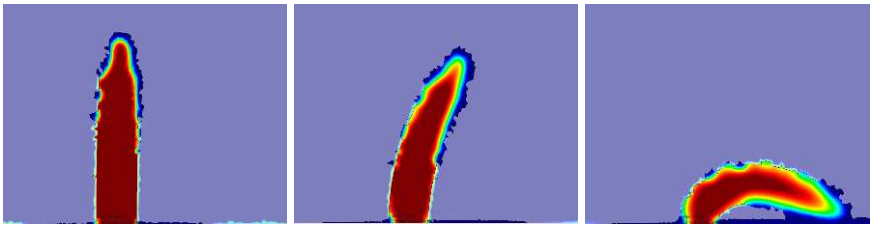

(a) $t = 28$ s (b) $t = 57$ s (c) $t = 105$ s

Fig. 20 Melting and dripping of a candle: viscosity evolution

Acknowledgements

M. Mier-Torrecilla thanks the Catalan Agency for Administration of University and Research Grants (AGAUR), the European Social Fund and CIMNE for their support.

Support from the European Commission and the European Research Council through the "Real Time Computational Techniques for Multi-Fluid Problems" project is also gratefully acknowledged.

References

1. Batchelor, G., *An Introduction to Fluid Dynamics*. Cambridge University Press, 1967.
2. Caboussat, A., Numerical simulation of two-phase free surface flows. *Archives of Computational Methods in Engineering* 12:165–224, 2005.
3. Carbonell, J., Modeling of ground excavation with the Particle Finite Element Method. Ph.D. Thesis, Universitat Politècnica de Catalunya, Barcelona (Spain), 2009.
4. Del Pin, F., Idelsohn, S., Oñate, E., Aubry, R., The ALE/Lagrangian Particle Finite Element Method: A new approach to computation of free-surfaces flows and fluid-object interactions. *Computers and Fluids* 36(1):27–38, 2007.
5. Drysdale, D., *An Introduction to Fire Dynamics*. Wiley Interscience, 1985.
6. Edelsbrunner, H., Mücke, E., Three-dimensional alpha shapes. *ACM Transactions on Graphics* 13:43–72, 1994.
7. Fernandez-Pello, A., Flame spread modeling. *Combustion Science and Technology* 39:119–134, 1984.
8. Gonzalez-Ferrari, C., El Método de los Elementos Finitos de Partículas: Aplicaciones a la pulvimetalurgia industrial. Ph.D. thesis, Universitat Politécnica de Catalunya, 2009.
9. Harlow, F., The Particle-in-Cell computing method for fluid dynamics. *Methods in Computational Physics* 3:313–343, 1964.
10. Hirt, C., Cook, J., Butler, T., A Lagrangian method for calculating the dynamics of an incompressible fluid with free surface. *Journal of Computational Physics* 5:103–124, 1970.
11. Hirt, C., Nichols, B., Volume of Fluid (VOF) method for the dynamics of free boundaries. *Journal of Computational Physics* 39:201–225, 1981.
12. Hughes, T., Liu, W., Zimmermann, T., Lagrangian-Eulerian finite element element formulation for incompressible viscous flows. *Computer Methods in Applied Mechanics and Engineering* 29:239–349, 1981.
13. Idelsohn, S., Calvo, N., Oñate, E., Polyhedrization of an arbitrary 3D point set. *Computer Methods in Applied Mechanics and Engineering* 192:2649–2667, 2003.
14. Idelsohn, S., Del Pin, F., Rossi, R., Oñate, E., Fluid-structure interaction problems with strong added-mass effect. *International Journal for Numerical Methods in Engineering* 80:1261–1294, 2009.
15. Idelsohn, S., Marti, J., Limache, A., Oñate, E., Unified Lagrangian formulation for elastic solids and incompressible fluids: Application to fluid-structure interaction problems via the PFEM. *Computer Methods in Applied Mechanics and Engineering* 197:1762–1776, 2008.
16. Idelsohn, S., Marti, J., Souto-Iglesias, A., Oñate, E., Interaction between an elastic structure and free-surface flows: Experimental versus numerical comparisons using the PFEM. *Computational Mechanics* 43:125–132, 2008.
17. Idelsohn, S., Mier-Torrecilla, M., Nigro, N., Oñate, E., On the analysis of heterogeneous fluids with jumps in the viscosity using a discontinuous pressure field. *Computational Mechanics*, 2009 (in press).
18. Idelsohn, S., Mier-Torrecilla, M., Oñate, E., Multi-fluid flows with the Particle Finite Element Method. *Computer Methods in Applied Mechanics and Engineering* 198:2750–2767, 2009.
19. Idelsohn, S., Oñate, E., Del Pin, F., A Lagrangian meshless finite element method applied to fluid-structure interaction problems. *Computers and Structures* 81(8–11), 655–671, 2003.
20. Idelsohn, S., Oñate, E., Del Pin, F., The Particle Finite Element Method: A powerful tool to solve incompressible flows with free-surfaces and breaking waves. *International Journal for Numerical Methods in Engineering* 61(7):964–989, 2004.

21. Idelsohn, S., Oñate, E., Del Pin, F., Calvo, N., Fluid-structure interaction using the Particle Finite Element Method. *Computer Methods in Applied Mechanics and Engineering* 195(17–18):2100–2123, 2006.
22. Idelsohn, S., Storti, M., Oñate, E., Lagrangian formulations to solve free surface incompressible inviscid fluid flows. *Computer Methods in Applied Mechanics and Engineering* 191(6–7):583–593, 2001.
23. Larese, A., Rossi, R., Oñate, E., Idelsohn, S., Validation of the Particle Finite Element Method (PFEM) for simulation of free surface flows. *Engineering Computations* 25:385–425, 2008.
24. Mier-Torrecilla, M., Numerical simulation of multi-fluid flows with the Particle Finite Element Method. Ph.D. Thesis, Technical University of Catalonia, 2010.
25. Mier-Torrecilla, M., Geyer, A., Phillips, J., Idelsohn, S., Oñate, E., Numerical simulations of negatively buoyant jets in an immiscible fluid using the Particle Finite Element Method. *Journal of Fluid Mechanics*, 2010 (submitted).
26. Mier-Torrecilla, M., Idelsohn, S., Oñate, E., A pressure segregation method for the Lagrangian simulation of interfacial flows. *International Journal for Numerical Methods in Fluids*, 2010 (submitted).
27. Oliver, J., Cante, J., Weyler, R., González, C., Hernández, J., Particle finite element methods in solid mechanics problems. In: *Computational Plasticity*, Vol. 1, pp. 87–103, Springer Verlag, 2007.
28. Oñate, E., Idelsohn, S., Celigueta, M., Rossi, R., Advances in the Particle Finite Element Method for the analysis of fluid-multibody interaction and bed erosion in free surface flows. *Computer Methods in Applied Mechanics and Engineering* 197:1777–1800, 2008.
29. Oñate, E., Idelsohn, S., Del Pin, F., Aubry, R., The Particle Finite Element Method: An overview. *International Journal of Computational Methods* 1(2):267–307, 2004.
30. Oñate, E., Rossi, R., Idelsohn, S., Butler, K., Melting and spread of polymers in fire with the Particle Finite Element Method. *International Journal for Numerical Methods in Engineering* 81:1046–1072, 2009.
31. Osher, S., Sethian, J., Fronts propagating with curvature dependant speed: algorithms based on Hamilton–Jacobi formulations. *Journal of Computational Physics* 79:12–49, 1988.
32. Poinsot, T., Veynante, D., *Theorical and Numerical Combustion*. Edwards, 2001.
33. Ramaswamy, B., Kawahara, M., Arbitrary Lagrangian-Eulerian finite element method for the analysis of free surface fluid flows. *Computational Mechanics* 1:103–108, 1986.
34. Ramaswamy, B., Kawahara, M., Lagrangian finite element analysis applied to viscous free surface fluid flow. *International Journal for Numerical Methods in Fluids* 7:953–984, 1987.
35. Rossi, R., Ryzhakov, P., Oñate, E., A monolithic FE formulation for the analysis of membranes in fluids. *International Journal of Space Structures* 24:205–210, 2009.
36. Scardovelli, R., Zaleski, S., Direct Numerical Simulation of free-surface and interfacial flow. *Annual Reviews of Fluid Mechanics* 31:567–603, 1999.
37. Shyy, W., *Computational Fluid Dynamics with Moving Boundaries*. Taylor & Francis, 1996.
38. Tezduyar, T., Behr, M., Liou, J., A new strategy for finite element computations involving moving boundaries and interfaces. The deforming-spatial-domain/space-time procedure: I. The concept and preliminary numerical tests. *Computer Methods in Applied Mechanics and Engineering* 94:339–351, 1992.
39. Tezduyar, T., Behr, M., Mittal, S., Liou, J., A new strategy for finite element computations involving moving boundaries and interfaces. The deforming-spatial-domain/space-time procedure: II. Computation of free-surface flows, two-liquid flows and flows with drifting cylinders. *Computer Methods in Applied Mechanics and Engineering* 94:353–371, 1992.
40. Unverdi, S., Tryggvason, G., Computations of multi-fluid flows. *Physica D: Nonlinear Phenomena* 60:70–83, 1992.
41. Unverdi, S., Tryggvason, G., A front-tracking method for viscous, incompressible, multi-fluid flows. *Journal of Computational Physics* 100:25–37, 1992.
42. Xie, W., DesJardin, P., An embedded upward flame spread model using 2D direct numerical simulations. *Combustion and Flame* 156:522–530, 2009.